

Wide-Band Tuneability, Nonlinear Transmission, and Dynamic Multistability in SQUID Metamaterials

G. P. Tsironis, N. Lazarides, I. Margaritis

Crete Center for Quantum Complexity and Nanotechnology, Department of Physics,
University of Crete, P.O. Box 2208, 71003 Heraklion, Greece

&

Institute of Electronic Structure and Laser,
Foundation for Research and Technology-Hellas, P.O. Box 1527, 71110 Heraklion, Greece
*corresponding author, E-mail: nl@physics.uoc.gr

Abstract

Superconducting metamaterials comprising rf SQUIDs (Superconducting QUantum Interference Devices) have been recently realized and investigated with respect to their tuneability, permeability and dynamic multistability properties. These properties are a consequence of intrinsic nonlinearities due to the sensitivity of the superconducting state to external stimuli. SQUIDs, made of a superconducting ring interrupted by a Josephson junction, possess yet another source of nonlinearity, which makes them widely tuneable with an applied dc flux. A model SQUID metamaterial, based on electric equivalent circuits, is used in the weak coupling approximation to demonstrate the dc flux tuneability, dynamic multistability, and nonlinear transmission in SQUID metamaterials comprising non-hysteretic SQUIDs. The model equations reproduce the experimentally observed tuneability patterns, and predict tuneability with the power of an applied ac magnetic field. Moreover, the results indicate the opening of nonlinear frequency bands for energy transmission through SQUID metamaterials, for sufficiently strong ac fields.

1. Introduction

Superconducting metamaterials [1], a particular class of artificial media that rely on the extraordinary properties of superconductors at sufficiently low temperatures, have been recently attracted great attention (see e.g., reference [2]). Conventional metamaterials, that comprise highly conducting metallic elements [3, 4, 5], typically exhibit high losses in the frequency range where their unusual and sought properties are manifested. The key element for the construction of conventional (metallic) metamaterials has customarily been the split-ring resonator (SRR), typically a highly conducting metallic ring with a slit, that can be regarded as an inductive-capacitive (LC) resonant oscillator. Nonlinearity, provided by combination of SRRs with electronic components (e.g., diodes [6]), adds a new degree of freedom for the design of tuneable metamaterials. Superconductors, on the other hand, are intrinsically nonlinear materials, due to the extreme sensitivity of the superconducting state in external stimuli [7, 8], which moreover exhibit significantly

reduced Ohmic losses. They thus provide unique opportunities to the researchers in the field for the fabrication of superconducting metamaterials with highly controllable effective electromagnetic properties including wideband tuneability [9, 10, 11, 12, 13, 14, 15, 16, 17, 18, 19, 20].

The direct superconducting analogue of a nonlinear SRR is the rf SQUID (rf Superconducting QUantum Interference Device), a long-known device in community of superconductivity. It consists of a superconducting ring interrupted by a Josephson junction (JJ) Josephson junction (JJ) [21], as shown schematically in figure 1(a). The SQUID is a strongly nonlinear resonator [22, 23], that is tuneable over a wide frequency range by applying either a flux bias [18, 24] or by varying the incoming rf power of an applied alternating field [24, 25]. This superconducting device has found up to date numerous applications [26, 27, 28, 29], and it is known to be the worlds most sensitive detector of magnetic signals. The replacement of metallic SRRs with rf SQUIDs, which have no direct electrical conduct but instead they are coupled magnetically through their mutual inductances, has been suggested theoretically a few years ago [30, 31]. Such SQUID metamaterials have been recently realized in the lab [18, 19, 32, 24, 25], that exhibit strong nonlinearities and wide-band tuneability with unusual magnetic properties due to macroscopic quantum effects. Nonlinearity and discreteness in SQUID metamaterials, along with low Ohmic losses (at least at microwave frequencies) may also lead in the generation of discrete breathers [33, 34, 35], i.e., time-periodic and spatially localized modes that change locally the magnetic response. Recent advances that led to nano-SQUIDs makes possible the fabrication of SQUID metamaterials at the nanoscale [36] (and references therein).

Superconducting metamaterials, resulting either from bare replacement of the metallic parts employed in conventional metamaterials by superconducting ones [37, 12, 11, 38, 39, 40, 41, 42], or by constructing hybrid structures comprising superconducting components [43, 44, 45, 46, 47, 48, 14, 49], or even by incorporating the Josephson effect as in arrays of SQUIDs [50, 18, 19, 32, 24], have been already proposed and/or demonstrated experimentally. Their operation frequency spans a huge range, from zero

[51, 52, 53, 54] to microwaves [55, 18, 56, 19, 32] and to Terahertz [11, 12, 37, 57, 38, 39, 40, 15, 58, 59, 41, 42] and visible [45] frequencies. Moreover, researchers rely on particular superconducting devices to access the truly quantum metamaterial regime [30, 60, 61, 62, 63].

In the present work, numerical calculations that rely on a model SQUID metamaterial in the weak coupling approximation are shown to reproduce fairly well the experimentally observed tuneability patterns with an applied constant (dc) flux bias. Specifically, it is demonstrated that the frequency band of linear flux waves of a SQUID metamaterial can be tuned periodically with the dc flux, with a period of one flux quantum. These results in a sense validate the discrete model. Quantitative differences in the tuneability patterns are attributed to the system size, dimensionality, nonlinearity strength (equivalently the amplitude of an applied rf alternating magnetic field), and coupling strength between neighboring SQUIDs. The transmission properties of SQUID metamaterials are investigated in the weakly nonlinear regime for a one-dimensional (1D) SQUID metamaterial with respect to the loss coefficient of the SQUIDs, for coupling strength which is in accordance with the weak coupling approximation (and in the range of values achieved in the experiments). For low losses and substantial nonlinearity, the transmission of flux waves through the metamaterial is also possible for frequencies outside the linear band, though the opening of one or more "channels" (i.e., nonlinear bands), whose effectiveness in transmitting energy depends on the nonlinearity strength.

2. SQUID Metamaterial Equations

Consider a two-dimensional (2D) rectangular lattice of identical SQUIDs in an ac and/or dc magnetic field, $\mathbf{H}(t)$, which is spatially uniform, as in figure 1(c). In the following we adopt the description (and notation) in references [35, 64], thus summarizing the essential building blocks of the model in a self-contained manner, yet omitting unnecessary details. The dynamic equations for the fluxes, $\phi_{n,m}$, in the (n, m) SQUID ring are given by [33, 34, 64]

$$\begin{aligned} & \ddot{\phi}_{n,m} + \gamma \dot{\phi}_{n,m} + \phi_{n,m} + \beta \sin(2\pi\phi_{n,m}) \\ & - \lambda_x(\phi_{n-1,m} + \phi_{n+1,m}) - \lambda_y(\phi_{n,m-1} + \phi_{n,m+1}) \\ & = [1 - 2(\lambda_x + \lambda_y)]\phi_{ext}, \quad (1) \end{aligned}$$

where the overdots denote differentiation with respect to the normalized time τ , λ_x and λ_y are the coupling coefficients in the x and y direction, respectively, $\beta = LL_c/\Phi_0 = \beta_L/2\pi$ is the rescaled SQUID parameter, and γ is a dimensionless coefficient representing all of the dissipation in each SQUID. The frequency and time in equation (1) are normalized to the corresponding LC SQUID frequency $\omega_0 = 1/\sqrt{LC}$ and its inverse ω_0^{-1} , respectively, while all fluxes are normalized to the flux quantum, Φ_0 . The external flux ϕ_{ext} is of the form

$$\phi_{ext} = \phi_{dc} + \phi_{ac} \cos(\Omega\tau), \quad (2)$$

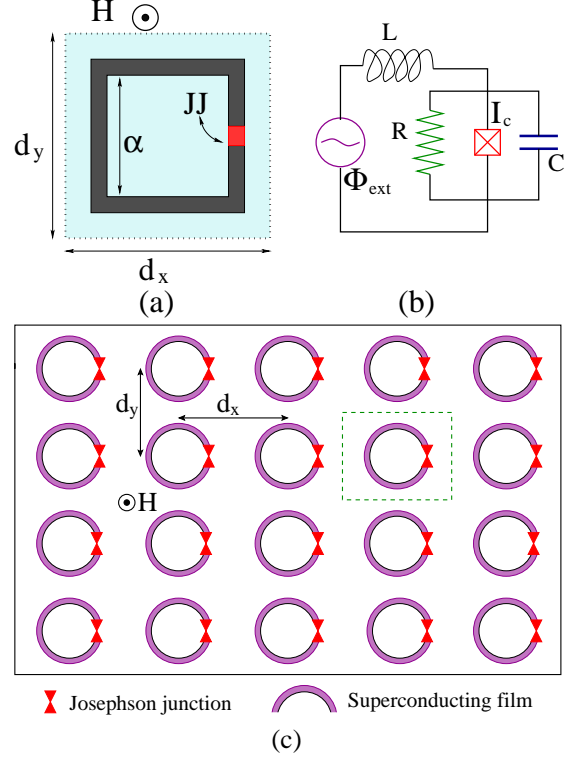


Figure 1: (color online) (a) Schematic drawing of an rf SQUID in a perpendicular time-dependent magnetic field $\mathbf{H}(t)$. (b) Equivalent electrical circuit (RCSJ model) for a single rf SQUID driven by a flux source Φ_{ext} . (c) Schematic drawing of a two-dimensional rf SQUID metamaterial, where the unit cell is indicated by the green-dashed line.

where Ω is the driving frequency, ϕ_{dc} is the flux bias, and ϕ_{ac} is the amplitude of the ac field. The current, $i_{n,m}$, flowing in the (n, m) SQUID, normalized to the critical current of the junction, I_c , is given by

$$\begin{aligned} i_{n,m} = \frac{1}{\beta} \{ & \phi_{n,m} - \phi_{eff} - \lambda_x(\phi_{n-1,m} + \phi_{n+1,m}) \\ & - \lambda_y(\phi_{n,m-1} + \phi_{n,m+1}) \}. \quad (3) \end{aligned}$$

For later use, the total maximum current per SQUID of the SQUID metamaterial is defined as

$$i_{max} = \max \left\{ \frac{1}{N_x N_y} \sum_{n,m=1}^{N_x, N_y} i_{n,m} \right\}_T, \quad (4)$$

i.e., the maximum value of the total current (given by the expression in the curly brackets) in one driving period $T = 2\pi/\Omega$. The SQUID metamaterial supports linear flux waves which frequency dispersion is

$$\Omega \equiv \Omega_\kappa = \sqrt{1 + \beta_L - 2(\lambda_x \cos \kappa_x + \lambda_y \cos \kappa_y)}, \quad (5)$$

where $\kappa = (\kappa_x, \kappa_y)$ is the normalized wavevector.

The dynamic behavior of rf SQUIDs has been investigated extensively for more than two decades, both in

the hysteretic ($\beta_L > 1$) and the non-hysteretic ($\beta_L < 1$) regimes. Just as conventional metamaterials acquire their properties from their individual elements, SQUID metamaterials acquire their resonance properties from individual SQUIDs. For very low amplitude of the ac driving field (linear regime), an rf SQUID exhibits a resonant magnetic response at a particular frequency

$$\omega_{SQ} = \omega_0 \sqrt{1 + \beta_L}, \quad (6)$$

which is always larger than its corresponding LC frequency, ω_0 . Tuneability of an rf SQUID can be achieved either with the amplitude of the ac field, ϕ_{ac} , or with the flux bias, ϕ_{dc} , which generate the flux threading its loop [35]. The resonance shift due to a dc flux bias has been actually observed in low- T_c , single rf SQUIDs in the linear regime [18], as well as in 1D SQUID metamaterials [19, 32, 56]. Assuming isotropic coupling, i.e., $\lambda_x = \lambda_y = \lambda$, the maximum and minimum values of the linear frequency band are then obtained by substituting $\kappa = (\kappa_x, \kappa_y) = (0, 0)$ and (π, π) , respectively, into equation (5). Thus we get

$$\omega_{max} = \sqrt{1 + \beta_L + 4|\lambda|}, \quad \omega_{min} = \sqrt{1 + \beta_L - 4|\lambda|}, \quad (7)$$

that give an approximate bandwidth $\Delta\Omega \simeq 4|\lambda|/\Omega_{SQ}$, where

$$\Omega_{SQ} = \frac{\omega_{SQ}}{\omega_0} = \sqrt{1 + \beta_L}. \quad (8)$$

The dynamic equations (1) are integrated with a fourth-order Runge-Kutta algorithm with fixed time-stepping, and the total energy of the SQUID metamaterial, in units of the Josephson energy E_J , is calculated from the expression

$$\begin{aligned} E_{tot} = \sum_{n,m} \left\{ \frac{\pi}{\beta} \left[\dot{\phi}_{n,m}^2 + (\phi_{n,m} - \phi_{ext})^2 \right] \right. \\ \left. + [1 - \cos(2\pi\phi_{n,m})] \right. \\ \left. - \frac{\pi}{\beta} [\lambda_x(\phi_{n,m} - \phi_{ext})(\phi_{n-1,m} - \phi_{ext}) \right. \\ \left. + \lambda_x(\phi_{n+1,m} - \phi_{ext})(\phi_{n,m} - \phi_{ext}) \right. \\ \left. + \lambda_y(\phi_{n,m-1} - \phi_{ext})(\phi_{n,m} - \phi_{ext}) \right. \\ \left. + \lambda_y(\phi_{n,m} - \phi_{ext})(\phi_{n,m+1} - \phi_{ext}) \right\}. \quad (9) \end{aligned}$$

The averaged energy in one driving period $T = 2\pi/\omega$ of evolution then reads

$$\langle E_{tot} \rangle_T = \frac{1}{T} \int_0^T d\tau E_{tot}(\tau), \quad (10)$$

where $\omega = \omega_0\Omega$ is the frequency of the applied ac flux.

3. dc flux tuneability

At frequencies within a narrow band, the metamaterial absorbs a large amount of energy. For dc flux bias equal to integer multiples of Φ_0 (including zero), that band coincides with the linear flux-wave band given in equation (5). However, for any other value of the dc flux, that band shifts downwards, down to a minimum attained for dc flux bias

equal to odd semi-integer multiples of Φ_0 . This procedure results in a very clear pattern of periodic shifting of the linear band with the dc flux bias, which has been observed in experiments [19, 32, 24]. Here the basic features of the dc flux tuneability patterns are reproduced by integrating equations (1) and using the calculated fluxes $\phi_{n,m}$ and voltages $\dot{\phi}_{n,m}$ to obtain the averaged energy per period of the ac field $\langle E_{tot} \rangle_T = \langle E_{tot} \rangle_T(\Omega = 2\pi/T, \phi_{dc})$ from equations (9) and (10) as a function of the frequency of the ac field Ω and the dc flux ϕ_{dc} . The quantity $\langle E_{tot} \rangle_T(\Omega =, \phi_{dc})$ is then presented in density plots on the $\Omega - \phi_{dc}$ plane in figure 2, for several combinations of ac flux amplitudes ϕ_{ac} and coupling coefficients λ . In these plots, the regions of resonant absorption correspond to maxima in the averaged energy, which appear as minima in the corresponding plots obtained from experiments, where the measured quantity is the frequency-dependent complex transmission amplitude $|S_{21}(\Omega)|$. In figure 2, while the dc flux is measured in units of Φ_0 , the frequencies has been transformed in natural units (GHz); the single-SQUID resonance frequency is chosen to be $f_{SQ} = 15 GHz$. The frequency f_{SQ} can be either calculated from the SQUID parameters or measured experimentally. The chosen value for f_{SQ} is slightly higher than the one measured in reference [25] for similar SQUID parameters; no attempt for an accurate fitting of the experimental data was made in this work. In figure 2, the ac amplitude ϕ_{ac} increases from left to right, while the coupling λ increases from top to bottom. Apparently, the resonant energy absorption, indicated by the dark regions, become stronger as one moves from left to right (increasing ϕ_{ac}), since the nonlinear effects become more and more important. When going from top to bottom panels, a smearing of the resonance is observed with increasing $|\lambda|$, along with the appearance of secondary resonances. The latter manifest themselves as thin dark curves that are located close to the main shifting pattern, and they are better seen around half-intefger values of the applied dc flux. The thickness of the low-transmission (dark) region in the close-to-linear regime, roughly corresponds to the width of the linear band, i.e., $\Delta\Omega \simeq 4|\lambda|/\Omega_{SQ}$.

These tuneability patterns can be understood within an approximate treatment valid for $\phi_{ac} \ll 1$. First assume that $\phi_{n,m} \simeq \phi$ for any n, m , i.e., that the SQUIDs are synchronized [64]; small deviations from complete synchronization arise due to the finite size of the metamaterial. We also assume that $\gamma \simeq 0$. Substitution into equations (1) and using equation (2), we get

$$\ddot{\phi} + (1 - 4\lambda)\dot{\phi} + \beta \sin(2\pi\phi) = (1 - 4\lambda)[\phi_{dc} + \phi_{ac} \cos(\Omega\tau)]. \quad (11)$$

In the earlier equation we further make the approximation

$$\beta \sin(2\pi\phi) \simeq \beta_L \phi - \frac{2\pi^2}{3} \beta_L \phi^3, \quad (12)$$

and the ansatz

$$\phi = \phi_0 + \phi_1 \cos(\Omega\tau), \quad (13)$$

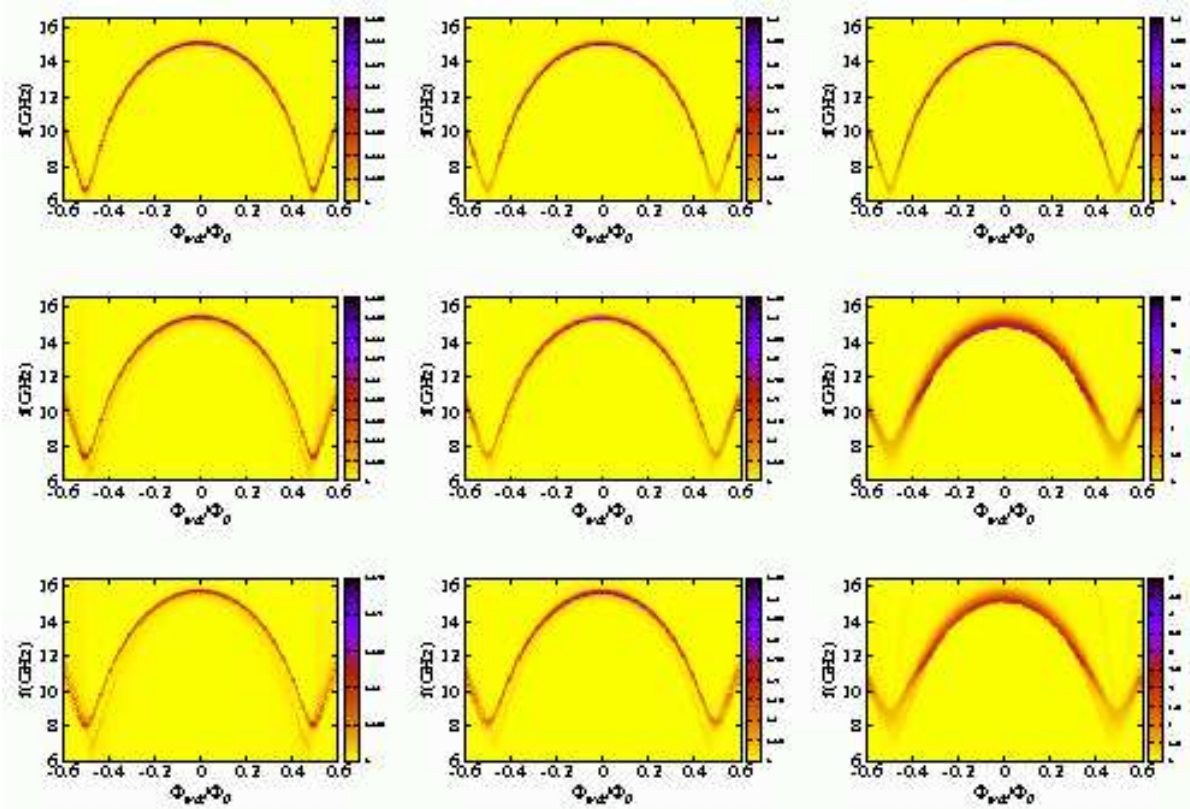


Figure 2: (color online) Density plot of the averaged total energy, $\langle E_{tot} \rangle_T$ as a function of the dc flux bias $\phi_{dc} = \Phi_{dc}/\Phi_0$ and the ac frequency f , for $N_x = N_y = 11$, $\beta_L \simeq 0.7$, $\gamma = 0.009$, and several combinations of ac amplitude $\phi_{ac} = \Phi_{ac}/\Phi_0$ and coupling coefficients λ . The driving ac amplitude increases from left to right, while the coupling increases from top to bottom. First column: $\lambda_x = \lambda_y = -0.01$, and $\phi_{ac} = 1/5000$ (left); $1/1000$ (middle); $1/200$ (right). Second column: $\lambda_x = \lambda_y = -0.03$, and $\phi_{ac} = 1/5000$ (left); $1/1000$ (middle); $1/200$ (right). Third column: $\lambda_x = \lambda_y = -0.05$, and $\phi_{ac} = 1/5000$ (left); $1/1000$ (middle); $1/200$ (right). The single-SQUID resonance frequency f_{SQ} used in the calculations is 15 GHz .

Substituting equations (12) and (13) into equation (11), using the rotating wave approximation (RWA), and separating constant from time-dependent terms, we get

$$\frac{2\pi^2}{3}\beta_L\phi_0^3 - (1 - 4\lambda + \beta_L)\phi_0 - \frac{3}{2}\phi_0\phi_1^2 + (1 - 4\lambda)\phi_{dc} = 0, \quad (14)$$

$$\frac{\pi^2}{2}\beta_L\phi_1^3 - \{(1 - 4\lambda + \beta_L - \Omega^2) - 2\pi^2\beta_L\phi_0^2\}\phi_1 + (1 - 4\lambda)\phi_{ac} = 0. \quad (15)$$

Limiting ourselves in the case $\phi_1 < \phi_0 \ll 1$, we may simplify equations (14) and (15), by neglecting terms proportional to ϕ_1^3 , ϕ_0^3 , and $\phi_0\phi_1^2$. Note that we keep the term $\propto \phi_0^2\phi_1$, i.e., the lowest order coupling term between the two equations. Then, the resulting equations can be easily solved to give

$$\phi_0 = \frac{(1 - 4\lambda)\phi_{dc}}{(\Omega_{SQ}^2 - 4\lambda)}; \quad (16)$$

$$\phi_1 = \frac{(1 - 4\lambda)\phi_{ac}}{\{(\Omega_{SQ}^2 - 4\lambda - \Omega^2) - 2\pi^2\beta_L\phi_0^2\}}. \quad (17)$$

Obviously, the ac flux amplitude in the SQUIDS, ϕ_1 , attains its maximum value when the expression in the curly brackets in the denominator of equation (17) is zero. Solving for Ω , we get

$$\Omega = \sqrt{(\Omega_{SQ}^2 - 4\lambda) - (2\pi^2\beta_L)\frac{(1 - 4\lambda)^2\phi_{dc}^2}{(\Omega_{SQ}^2 - 4\lambda)^2}}, \quad (18)$$

or, in natural units

$$f = \frac{f_{SQ}}{\Omega_{SQ}} \sqrt{(\Omega_{SQ}^2 - 4\lambda) - (2\pi^2\beta_L)\frac{(1 - 4\lambda)^2\phi_{dc}^2}{(\Omega_{SQ}^2 - 4\lambda)^2}}, \quad (19)$$

which corresponds to the "resonance frequency" of the SQUID metamaterial itself, with f_{SQ} is the single-SQUID resonance frequency. From the data of the tuneability patterns presented in the left column of figure 2 (weak driving amplitude), that correspond to increasing coupling from top to bottom, we have extracted the frequency of maximum response by simply identifying the frequency where the total energy is maximum. A typical curve of this kind is shown in figure 3, along with the corresponding one calculated from equation (18). This is the case of low-amplitude ac driving,

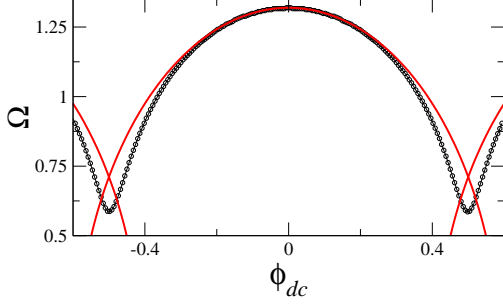


Figure 3: (color online) Normalized frequency at maximum response of the SQUID metamaterial, Ω , as a function of the dc applied (normalized) flux, ϕ_{dc} , in the presence of a low-amplitude alternating signal. The black circles are obtained from the numerical simulations through model equations (1) (see text), while the red solid lines are plotted from the approximate equation (18). Parameters: $\lambda_x = \lambda_y = -0.01$, $N_x = N_y = 11$, $\phi_{ac} = 1/5000$, $\gamma = 0.009$, and $\beta_L \simeq 0.7$.

that is the closest to the assumptions made for the derivation of expression (18). It is remarkable that this simple expression, which contains only two parameters, λ and β_L , fairly agrees with the simulations in a rather wide region of dc fluxes, i.e., from $\phi_{dc} \sim -0.3$ to $\sim +0.3$. Within this interval, the normalized frequency in figure 3 changes from $\Omega = 1.12$ to 1.32 , that makes a tuneability range of 15%. This is approximately the "useful" tuneability range [19, 32], since at these frequencies the energy absorption remains at high levels (i.e., the resonance is strong). For larger ϕ_{dc} , the importance of the term $\propto \phi_0^3$ increases and it cannot be neglected for the solutions of equations (14) and (15). The approximate expression (18) also captures another experimentally observed feature, namely the increase of the metamaterial resonance frequency at zero dc flux, $f(\phi_{dc} = 0)$. By setting $\phi_{dc} = 0$ in equation (18) we get that $f = \frac{f_{SQ}}{\Omega_{SQ}} \sqrt{(\Omega_{SQ}^2 - 4\lambda)}$, which, for $f_{SQ} = 15 \text{ GHz}$, $\Omega_{SQ} = 1.304$ ($\beta_L = 0.7$), $\lambda = -0.01, -0.03, -0.05$ gives respectively, $f = 15.2, 15.5, 15.9 \text{ GHz}$ in agreement with the numerical results. The λ -dependence of the SQUID metamaterial resonance frequency is weaker in the corresponding one-dimensional case. This effect does not however result directly from the nonlinearity; the ac field is very weak to induce significant nonlinear effects. Instead, it comes from the assumed uniformity of the SQUID metamaterial state, i.e., the assumption $\phi_{n,m} = \phi$ for any n, m . From that, and neglecting the dissipation and driving terms, we get the single eigenfrequency of the metamaterial in that state as $\Omega = \sqrt{\Omega_{SQ}^2 - 4\lambda}$, so that deviations of the resonance frequency from that of a single SQUID are approximately proportional to λ ($|\lambda| \ll 1$).

4. Energy Transmission through SQUID Metamaterial Lines.-

SQUID metamaterials support flux waves that are capable of transmitting energy, in much the same way as in nonlinear magnetoinductive transmission lines made of conventional (metallic) metamaterials [65], which may function as a frequency-selective communication channel for devices. For simplicity and clarity we use a one-dimensional SQUID metamaterial comprising $N = 54$ identical elements with $\beta_L = 0.7$ ($\beta = 0.1114$) weakly coupled to their nearest neighbors. In order to investigate the transfer of energy through the array, the SQUID that is located at the left end (i.e., that for $n = 1$) is excited by an ac flux field at a particular frequency. The system of equations (1) and equation (9) in the present case read

$$\ddot{\phi}_n + \gamma \dot{\phi}_n + \phi_n + \beta \sin(2\pi\phi_n) - \lambda(\phi_{n-1} + \phi_{n+1}) = (1 - 2\lambda)\phi_{ext} \delta_{n,1}, \quad (20)$$

where the coupling coefficient is now denoted by λ and the Kronecker's delta $\delta_{n,1}$ indicates that only the SQUID with $n = 1$ is driven by the ac field, and

$$E_{tot} = \sum_n \left\{ \frac{\pi}{\beta} \left[\dot{\phi}_n^2 + (\phi_n - \phi_{ext})^2 \right] + 1 - \cos(2\pi\phi_n) - \frac{\pi}{\beta} [\lambda(\phi_n - \phi_{ext})(\phi_{n-1} - \phi_{ext}) + \lambda(\phi_{n+1} - \phi_{ext})(\phi_n - \phi_{ext})] \right\} \quad (21)$$

Equations (20) implemented with the boundary conditions $\phi_0 = \phi_{N+1}$ are integrated in time for $12000 T$ time units, where $T = 2\pi/\Omega$ is the driving period, so that transient effects are eliminated and the system has reached a stationary state. The energy density in the metamaterial is then calculated from (21) as the average over the next $2000 T$ time units. The decimal logarithm of the averaged energy density is mapped on the frequency Ω - site number n plane (figure 4), where high transmission regions are indicated with darker colors. In figure 4, the changes in the energy transmission with respect to the dissipation coefficient γ are shown for fixed coupling coefficient $\lambda = -0.01$ and ac field $\phi_{ac} = 0.1$. Note that for that value of ϕ_{ac} , significant nonlinearity is already present.

The energy transmission map for relatively strong dissipation ($\gamma = 0.009$) is shown in the upper panel of figure 4. Significant energy transmission occurs in a narrow band, of the order $\sim 2\lambda$ around the single SQUID resonance frequency $\Omega_{SQ} \simeq 1.3$ (for $\beta_L = 0.7$). This band almost coincides with the linear band for the one-dimensional SQUID metamaterial. Note that energy transmission also occurs at other frequencies; e.g., at $\Omega \sim 0.43$ that corresponds to a subharmonic resonance. Subharmonic resonances result from nonlinearity; in this case, nonlinear effects are already significant due to the relatively high ac field amplitude ($\phi_{ac} = 0.1$). However, with decreasing losses (middle panel), more energy is transmitted both at frequencies in the linear band and the subharmonic resonance band. In

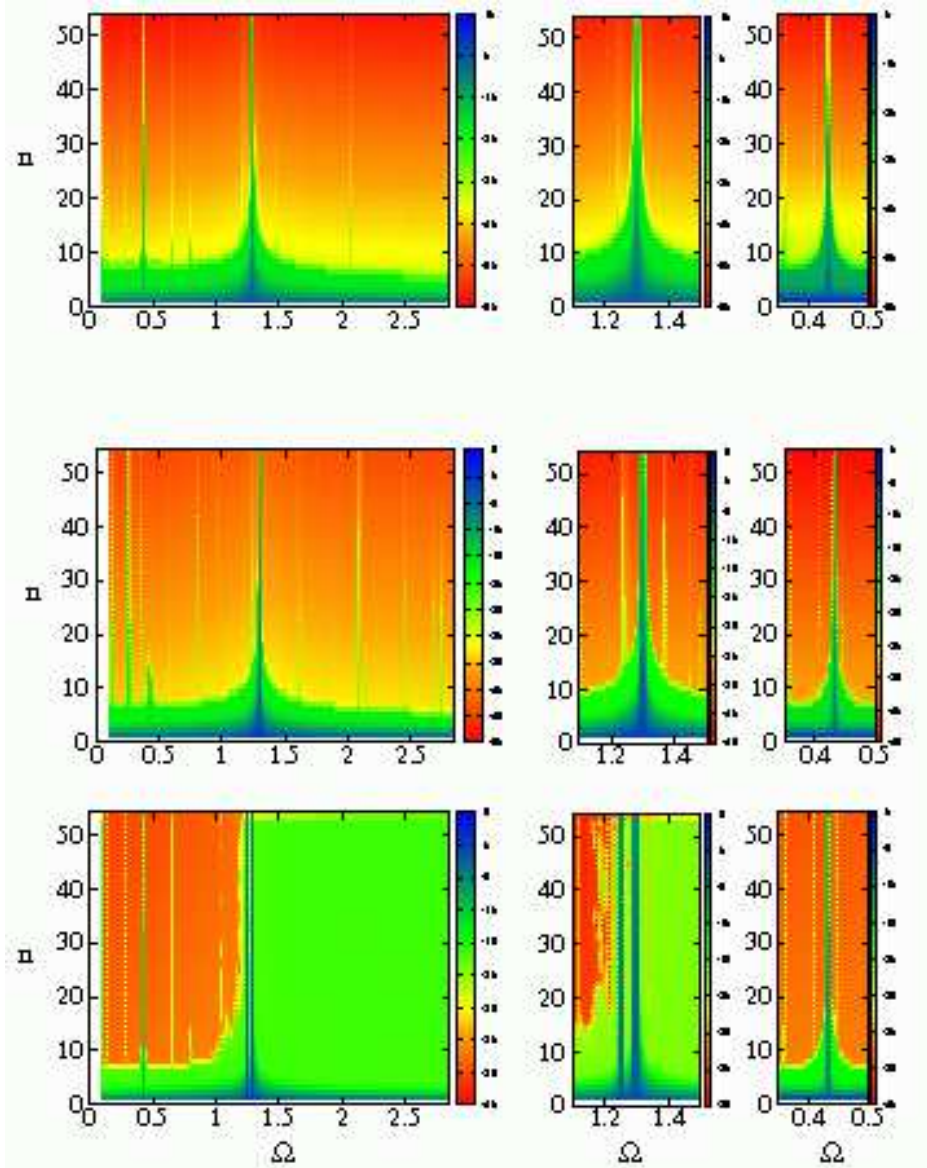


Figure 4: (color online) Energy transmission through a one-dimensional SQUID metamaterial line with $N = 54$ SQUIDs. The logarithm of the energy density averaged over $2000T$ time units, $\log_{10}[\langle E_n \rangle_T]$, is plotted on the site number n - driving frequency Ω plane for $\beta_L = 0.7$ ($\beta = 0.1114$), $\lambda = -0.01$, and $\gamma = 0.009$ (upper); $\gamma = 0.004$ (middle); $\gamma = 0.001$ (lower). The middle and left columns are enlargements in frequency ranges around the fundamental and the subharmonic resonance, respectively, at $\Omega \simeq 1.302$ and 0.43 .

the following we refer to the latter as the nonlinear band, since it results from purely nonlinear effects. With further decrease of losses (lower panel), the transmitted energy in these two bands becomes more significant. The comparison can be made more clearly by looking at the panels in the middle and right columns, which show enlarged regions of the corresponding panels shown in the left column. The enlargement around the linear band shown in the middle column shows clearly the increase of the transmitted energy with decreasing losses. Moreover, in the case of very low losses ($\gamma = 0.001$) the linear band splits into two bands, where significant energy transmission occurs. The energy transmission in the nonlinear band increases with decreas-

ing losses, accordingly (left column, losses decrease from top to bottom).

Thus, for sufficiently strong ac field, energy can be transmitted not only for frequencies in the linear band, but also in otherwise forbidden frequency regions. The metamaterial thus becomes transparent in energy transmission at frequency intervals around nonlinear resonances (subharmonic, in the present case) of single rf SQUIDs. That type of self-induced transparency due to nonlinearity is a robust effect as can be seen in figure 4, where the loss coefficient has been varied by almost an order of magnitude. In the density plots above, the right boundary was actually a reflecting one, that allows the formation of stationary states in

the array. However, the same calculations performed with a totally absorbing boundary give practically identical results.

For very low amplitude of the applied ac field ϕ_{ac} and $\phi_{dc} = 0$, equations (20) can be linearized to give

$$\begin{aligned} \ddot{\phi}_n + \gamma \dot{\phi}_n + \Omega_{SQ}^2 \phi_n - \lambda(\phi_{n-1} + \phi_{n+1}) \\ = \bar{\phi}_{ac} \cos(\Omega\tau) \delta_{n,1}, \end{aligned} \quad (22)$$

where $\bar{\phi}_{ac} = (1 - 2\lambda)\phi_{ac}$. If we further neglect the loss term, equations (22) can be solved exactly in closed form for any driving frequency Ω and for any finite N , the total number of SQUIDs in the one-dimensional array. By substitution of the trial solution $\phi_n = q_n \cos(\Omega\tau)$ into equations (22) and after some rearrangement we get

$$sq_{n-1} + q_n + sq_{n+1} = \kappa_0 \delta_{n,1}, \quad (23)$$

where

$$s = -\frac{\lambda}{\Omega_{SQ}^2 - \Omega^2}, \quad \kappa_0 = \frac{\bar{\phi}_{ac}}{\Omega_{SQ}^2 - \Omega^2}, \quad (24)$$

or, in matrix form

$$\mathbf{q} = \kappa_0 \hat{\mathbf{S}}^{-1} \mathbf{E}_1, \quad (25)$$

where \mathbf{q} and \mathbf{E}_1 are N -dimensional vectors with components q_n and $\delta_{n,1}$, respectively, and $\hat{\mathbf{S}}^{-1}$ is the inverse of the $N \times N$ coupling matrix $\hat{\mathbf{S}}$. The latter is a real, symmetric, tridiagonal matrix that has its diagonal elements equal to unity, while all the other non-zero elements are equal to s . The elements of the matrix $\hat{\mathbf{S}}^{-1}$ can be obtained in closed analytical form [66] using known results for the inversion of more general tridiagonal matrices [67]. Then, the components of the \mathbf{q} vector can be written as

$$q_n = \kappa_0 \left(\hat{\mathbf{S}}^{-1} \right)_{n,1}, \quad (26)$$

where $\left(\hat{\mathbf{S}}^{-1} \right)_{n,1}$ is the $(n, 1)$ -element of $\hat{\mathbf{S}}^{-1}$, whose explicit form is given in reference [66]. Then, the solution of the linear system (22) with $\gamma = 0$ is

$$\begin{aligned} \phi_n(\tau) = \kappa_0 \mu \frac{\sin[(N-n+1)\theta']}{\sin[(N+1)\theta']} \cos(\Omega\tau), \\ \theta' = \cos^{-1} \left(\frac{1}{2|s|} \right), \end{aligned} \quad (27)$$

for $s > +1/2$ and $s < -1/2$ (in the linear flux-wave band), and

$$\begin{aligned} \phi_n(\tau) = \kappa_0 \mu \frac{\sinh[(N-n+1)\theta]}{\sinh[(N+1)\theta]} \cos(\Omega\tau), \\ \theta = \ln \frac{1 + \sqrt{1 - (2s)^2}}{2|s|}, \end{aligned} \quad (28)$$

for $-1/2 < s < +1/2$ (outside the linear flux-wave band), where

$$\mu = \frac{1}{|s|} \left(-\frac{|s|}{s} \right)^{n-1}. \quad (29)$$

The above expressions actually provide the asymptotic solutions, i.e., after the transients due to dissipation, etc., have died out. Thus, these driven linear modes correspond to the stationary state of the linearized system; the dissipation however may alter somewhat their amplitude, without affecting very much their form. Note also that the q_n s are uniquely determined by the parameters of the system, and they vanish with vanishing ϕ_{ac} .

From the analytical solution at frequencies within the linear flux-wave band, equation (27) which corresponds to either $s > +1/2$ or $s < -1/2$, the resonance frequencies of the array can be obtained by setting $\sin[(N+1)\theta'] = 0$. Thus we get

$$s \equiv s_m = \frac{1}{2 \cos \left[\frac{m\pi}{(N+1)} \right]}, \quad (30)$$

where m is an integer ($m = 1, \dots, N$). By solving the first of equations (24) with respect to Ω , and substituting the values of $s \equiv s_m$ from equation (30) we get

$$\Omega \equiv \Omega_m = \sqrt{\Omega_{SQ}^2 + 2\lambda \cos \left(\frac{m\pi}{N+1} \right)}, \quad (31)$$

which is the discrete frequency dispersion for linear flux-waves in a one-dimensional SQUID metamaterial, with m being the mode number ($m = 1, \dots, N$).

5. Dynamic Multistability and Power-Dependent Tuneability.

The dc flux tuneability of SQUID metamaterials is a truly nonlinear effect, which appears also in the "linear regime", where the very low ac power levels allow for the treatment of a Josephson junction as a quasi-linear inductance. In figure 2 we have observed that with increasing ϕ_{ac} (increasing thus the significance of nonlinearity), the complexity of the tuneability patterns increases as well, while they exhibit high power absorption in a frequency range that exceeds the boundaries of the linear band. Thus, with increasing power, new dynamic effects are expected to appear; with resonance frequency shifts and multistability being the most prominent. The latter, in particular, is a purely dynamic phenomenon that is not related to the multistability known from hysteretic SQUIDs. For a particular choice of parameters, dynamic multistability manifests itself as a small number of simultaneously stable states. As it has been shown in recent experiments [18], each of these states corresponds to a different value of the SQUID magnetic flux susceptibility at the driving frequency, that may be either positive or negative. This implies that, depending on the state of individual SQUIDs, the metamaterial can either be magnetically almost transparent or not.

While in figure 2 the amplitude of the ac field was kept to low values (0.005 the highest), in the present section we use higher values. Due to the resonant nature of the SQUIDs, the current may attain values that are higher than the critical current of the Josephson junctions. In this case,

the standard RCSJ model gives unphysically high current values, because it does not take into account the change in the conductance of the junctions [23] (p. 48). In order to incorporate that change, we replace the dissipation coefficient γ in equations (1) with the following current dependent function

$$\gamma_{n,m} = \gamma_0 + c \left[1 + \tanh \left(\frac{i_{n,m} - 1}{d} \right) \right], \quad (32)$$

where $c = 0.12$, $d = 0.02$, and $\gamma_0 = 0.009$, the value of γ used for obtaining the results of figure 2. That function allows for an abrupt but continuous change of the dissipation coefficient from low values $\gamma_{n,m} \simeq \gamma_0$ (low current, less than I_c) to high values $\gamma_{n,m} \simeq 28\gamma_0$ (high current, greater than I_c). We have calculated several curves of the total current maximum i_{max} as a function of the driving frequency Ω , which are shown in figure 5. In this figure, the amplitude of the applied ac field increases from the bottom to the upper panel [from (f) to (a)]. In all subfigures, the frequency is varied between $\Omega \simeq 0.8 - 6.28$ in both increasing from the lowest frequency or decreasing from the highest frequency (only part of this range is shown). In this way we may identify two different branches of the $i_{max} - \Omega$ at a particular frequency range for relatively high ac powers. For low power of the ac field [figures 5(f)-5d] no hysteresis and thus multistability is observed. However, hysteretic effects appears in figure 5(c) for $\phi_{ac} = 0.03$ for a very narrow frequency interval. With further increasing ϕ_{ac} we see that the hysteretic lobe, and thus the frequency region of multistability, significantly increases [figures 5(b)-5(a)]. Besides the multistability effects, in figure 5 we also observe strong resonance red-shift with increasing ac power level. For low power levels [figure 5(f)] the curve exhibits a strong resonant response at $\sim \Omega_{SQ}$, the single SQUID (linear) resonance frequency. With increasing ac power, however, the resonance frequency, determined by the maximum of each curve, moves to lower frequencies. Note that in figures 5(b) and 5(a), there are frequency regions where the SQUID metamaterial jumps intermittently from the low to the high current state (or vice versa). In comparison with the standard RCSJ model, that nonlinear resistive Josephson junction model severely limits total maximum currents which are greater than the critical one; it also exhibit much less hysteretic effects, that are visible at relatively high powers only.

6. Conclusions.-

We have used a SQUID metamaterial model in the weak coupling approximation, in order to explore the tuneability, nonlinear transmission, and dynamic multistability properties of SQUID metamaterials. The numerical results reproduce very well the experimentally observed dc flux tuneability patterns, whose form remains qualitatively unaffected from the details of the particular SQUID metamaterial. System parameters such as the size of the system, its dimensionality, the SQUID parameter, and the coupling between SQUIDs, mainly affect the tuneability range (i.e.,

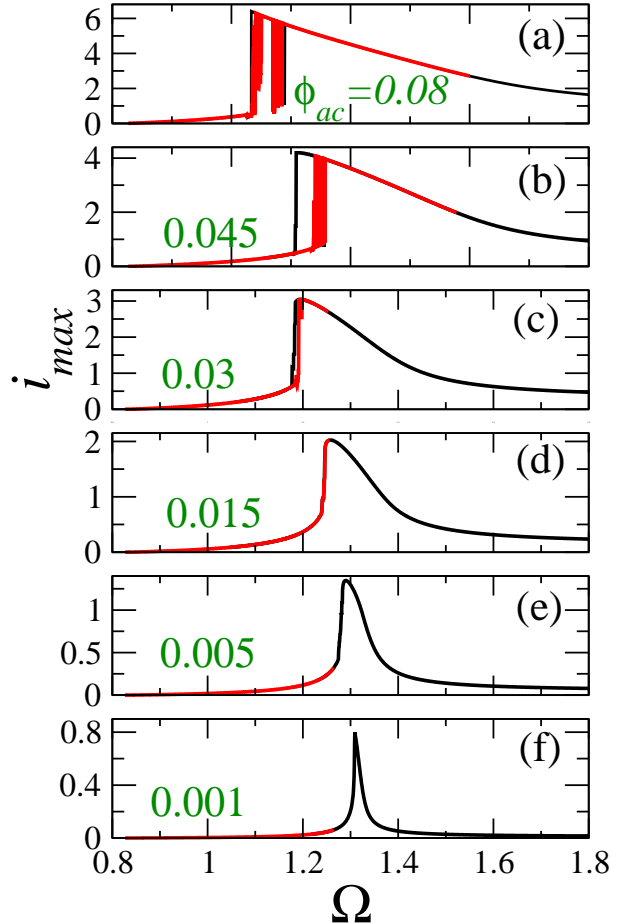


Figure 5: (color online) The maximum total current i_{max} in the SQUID metamaterial as a function of the normalized frequency Ω , for $N_x = N_y = 11$, $\lambda_x = \lambda_y = -0.01$, $\beta_L \simeq 0.7$, $\gamma_0 = 0.009$ (see text), $\phi_{dc} = 0$, and (a) $\phi_{ac} = 0.08$; (b) $\phi_{ac} = 0.045$; (c) $\phi_{ac} = 0.03$; (d) $\phi_{ac} = 0.015$; (e) $\phi_{ac} = 0.005$; (f) $\phi_{ac} = 0.001$.

the minimum and maximum value of resonance frequency of the metamaterial).

In the linear regime, a simple approximate expression which gives the dependence of the resonance frequency on the dc flux bias and the coupling strength can be obtained. Although it has been obtained under several simplifying assumptions, it agrees fairly well with the numerically obtained tuneability patterns within a significant tuneability range. This expression also explains the increase of the zero dc flux resonance frequency with increasing coupling strength, which comes from the excitation of a mode where all the SQUIDs are synchronized.

Simulations of one-dimensional SQUID metamaterials which are driven at one end, reveal their energy transmission properties. For low amplitude of the ac applied field, energy transmission is limited at frequencies within the linear band. In that case, the linearized equations can be solved exactly, and the amount of transmitted energy in each SQUID could be calculated (with a correction for slight reduction of energy due to dissipation which has been

neglected in the analytical calculations). For stronger ac fields, the nonlinear effects become significant, and significant amounts of energy can be transmitted through nonlinear frequency bands which appear due to secondary SQUID resonances.

The resonance of the maximum total current as a function of the driving frequency shifts to lower frequencies with increasing ac field amplitude. For relatively strong ac fields, dynamic bistability appears. For a more realistic description of the Josephson junctions in the SQUID metamaterial, the nonlinear variation of their resistance with current in each SQUID has been taken into account.

Acknowledgement

This work was partially supported by the European Union's Seventh Framework Programme (FP7-REGPOT-2012-2013-1) under grant agreement n^o 316165, and by the Thales Project MACOMSYS, cofinanced by the European Union (European Social Fund ESF) and Greek national funds through the Operational Program "Education and Lifelong Learning" of the National Strategic Reference Framework (NSRF) Research Funding Program: THALES. Investing in knowledge society through the European Social Fund.

References

- [1] S.M. Anlage, *J. Opt.* **13**, 024001 (2011)
- [2] in *Special Issue: Focus on Superconducting Metamaterials*, vol. 26, ed. by A.V. Ustinov, S. Anlage, A. Sanchez (Supercond. Sci. Technol., 2013)
- [3] D.R. Smith, J.B. Pendry, Wiltshire, *Science* **Vol. 305 no. 5685**, 788 (2004)
- [4] V.M. Shalaev, *Nature Photonics* **1**, 41 (2007)
- [5] C.M. Soukoulis, M. Wegener, *Nature Photonics* **5**, 523 (2011)
- [6] I.V. Shadrivov, A.B. Kozyrev, D.W. van der Weide, Y.S. Kivshar, *Appl. Phys. Lett.* **93**, 161903 (2008)
- [7] N.I. Zheludev, *Science* **328**, 582 (2010)
- [8] N.I. Zheludev, *Optics and Photonics News* **22**, 31 (2011)
- [9] M.C. Ricci, N. Orloff, S.M. Anlage, *Appl. Phys. Lett.* **87**, 034102 (2005)
- [10] M.C. Ricci, H. Xu, R. Prozorov, A.P. Zhuravel, A.V. Ustinov, S.M. Anlage, *IEEE Trans. Appl. Supercond.* **17**, 918 (2007)
- [11] H.T. Chen, H. Yang, R. Singh, J.F. OHara, A.K. Azad, A. Stuart, S.A. Trugman, Q.X. Jia, A.J. Taylor, *Phys. Rev. Lett.* **105**, 247402 (2010)
- [12] B. Jin, C. Zhang, S. Engelbrecht, A. Pimenov, J. Wu, Q. Xu, C. Cao, J. Chen, W. Xu, *Opt. Express* **18**, 17504 (2010)
- [13] V.A. Fedotov, A. Tsiatmas, J.H. Shi, R. Buckingham, P. de Groot, Y. Chen, S. Wang, N.I. Zheludev, *Opt. Express* **18**, 9015 (2010)
- [14] C. Kurter, P. Tassin, A.P. Zhuravel, L. Zhang, T. Koschny, A.V. Ustinov, C.M. Soukoulis, S.M. Anlage, *Appl. Phys. Lett.* **100**, 121906 (2012)
- [15] R. Singh, J. Xiong, A.K. Azad, H. Yang, S.A. Trugman, Q.X. Jia, A.J. Taylor, H.T. Chen, *Nanophotonics* **1**, 117123 (2012)
- [16] R. Singh, J. Xiong, D.R. Chowdhury, H. Yang, A.K. Azad, S.A. Trugman, Q.X. Jia, A.J. Taylor, H.T. Chen, *Proc. SPIE* **8423**, 84230Y (2012)
- [17] V. Savinov, V.A. Fedotov, S.M. Anlage, P.A.J. de Groot, N.I. Zheludev, *Phys. Rev. Lett.* **109**, 243904 (2012)
- [18] P. Jung, S. Butz, S.V. Shitov, A.V. Ustinov, *Appl. Phys. Lett.* **102**, 062601 (2013)
- [19] S. Butz, P. Jung, L.V. Filippenko, V.P. Koshelets, A.V. Ustinov, *Opt. Express* **29 (19)**, 22540 (2013)
- [20] D. Zueco, C. Fernández-Juez, J. Yago, U. Naether, B. Peropadre, J.J. García-Ripoll, J.J. Mazo, *Supercond. Sci. Technol.* **26**, 074006 (8pp) (2013)
- [21] B. Josephson, *Phys. Lett. A* **1**, 251 (1962)
- [22] A. Barone, G. Patternó, *Physics and Applications of the Josephson Effect*. (Wiley, New York, 1982)
- [23] K.K. Likharev., *Dynamics of Josephson Junctions and Circuits*. (Gordon and Breach, Philadelphia, 1986)
- [24] M. Trepanier, D. Zhang, O. Mukhanov, S.M. Anlage, arXiv:1308.1410 (2013)
- [25] P. Jung, S. Butz, M. Marthaler, M.V. Fistul, J. Leppäkangas, V.P. Koshelets, A.V. Ustinov, arXiv:1312.2937 (2013)
- [26] W.G. Jenks, S.S.H. Sadeghi, J.P.W. Jr, *J. Phys. D: Appl. Phys.* **30**, 293 (1997)
- [27] D. Koelle, R. Kleiner, F. Ludwig, E. Dantsker, J. Clarke, *Rev. Mod. Phys.* **71**, 631 (1999)
- [28] R. Kleiner, D. Koelle, F. Ludwig, J. Clarke, *Proceedings of the IEEE* **92**, 1534 (2004)
- [29] R.L. Fagaly, *Review of Scientific Instruments* **77**, 101101 (2006)
- [30] C. Du, H. Chen, S. Li, *Phys. Rev. B* **74**, 113105 (2006)
- [31] N. Lazarides, G.P. Tsironis, *Appl. Phys. Lett.* **16**, 163501 (2007)

- [32] S. Butz, P. Jung, L.V. Filippenko, V.P. Koshelets, A.V. Ustinov, *Supercond. Sci. Technol.* **26**, 094003 (2013)
- [33] N. Lazarides, G.P. Tsironis, M. Eleftheriou, *Nonlinear Phenom. Complex Syst.* **11**, 250 (2008)
- [34] G.P. Tsironis, N. Lazarides, M. Eleftheriou, *PIERS Online* **5**, 26 (2009)
- [35] N. Lazarides, G.P. Tsironis, *Proc. SPIE* **8423**, 84231K (2012)
- [36] W. Wernsdorfer, *Supercond. Sci. Technol.* **22**, 064013 (2009)
- [37] J. Gu, R. Singh, Z. Tian, W. Cao, Q. Xing, M.X. He, J.W. Zhang, J. Han, H. Chen, W. Zhang, *Appl. Phys. Lett.* **97**, 071102 (2010)
- [38] C.H. Zhang, J.B. Wu, B.B. Jin, Z.M. Ji, L. Kang, W.W. Xu, J. Chen, M. Tonouchi, P.H. Wu, *Opt. Express* **20** (1), 42 (2011)
- [39] J.B. Wu, B.B. Jin, J. Wan, L. Liang, Y.G. Zhang, T. Jia, C.H. Cao, L. Kang, W.W. Xu, J. Chen, P.H. Wu, *Appl. Phys. Lett.* **99**, 161113 (2011)
- [40] C.H. Zhang, J.B. Wu, B.B. Jin, Z.M. Ji, L. Kang, W.W. Xu, J. Chen, M. Tonouchi, P.H. Wu, *Opt. Express* **20** (1), 42 (2012)
- [41] C.H. Zhang, J.H. B. B. Jin, I. Kawayama, H. Murakami, X. Jia, L. Liang, L. Kang, J. Chen, P. Wu, M. Tonouchi, *New Journal of Physics* **15**, 055017 (2013)
- [42] B.B. Jin, C. H. Zhang, J. Han, I. Kawayama, H. Murakami, J.B. Wu, L. Kang, J. Chen, P.H. Wu, M. Tonouchi, *Appl. Phys. Lett.* **102**, 081121 (2013)
- [43] A. Pimenov, A. Loidl, P. Przyslupski, B. Dabrowski, *Phys. Rev. Lett.* **95**, 247009 (2005)
- [44] A.G. Kussow, A. Akyurtlu, A. Semichaevsky, N. Angkawisittpan, *Phys. Rev. B* **76**, 195123 (2007)
- [45] N. Limberopoulos, A. Akyurtlu, K. Higginson, A.G. Kussow, C.D. Merritt, *Appl. Phys. Lett.* **95**, 023306 (2009)
- [46] A.L. Rakhmanov, V.A. Yampolskii, J.A. Fan, F. Caspasso, F. Nori, *Phys. Rev. B* **81** (7), 075101 (2010)
- [47] V.A. Golick, D.V. Kadygrob, V.A. Yampolskii, A.L. Rakhmanov, B.A. Ivanov, F. Nori, *Phys. Rev. Lett.* **104**, 187003 (2010)
- [48] C. Kurter, P. Tassin, L. Zhang, T. Koschny, A.P. Zhuravel, A.V. Ustinov, S.M. Anlage, C.M. Soukoulis, *Phys. Rev. Lett.* **107**, 043901 (2011)
- [49] J. Prat-Camps, A. Sanchez, C. Navau, *Supercond. Sci. Technol.* **26**, 074001 (2013)
- [50] M.A. Castellanos-Beltran, K.D. Irwin, G.C. Hilton, L.R. Vale, K.W. Lehnert, *Nature Physics* **4**, 928 (2008)
- [51] F. Magnus, B. Wood, J. Moore, K. Morrison, G. Perkins, J. Fyson, M.C.K. Wiltshire, D. Caplini, L.F. Cohen, J.B. Pendry, *Nature Mater.* **7**, 295 (2008)
- [52] C. Navau, D.X. Chen, A. Sanchez, N. Del-Valle, *Appl. Phys. Lett.* **94** (24), 242501 (2009)
- [53] Y. Mawatari, C. Navau, A. Sanchez, *Phys. Rev. B* **85**, 134524 (2012)
- [54] Y. Mawatari, *Supercond. Sci. Technol.* **26**, 074005 (2013)
- [55] C. Kurter, J. Abrahams, S.M. Anlage, *Appl. Phys. Lett.* **96**, 253504 (2010)
- [56] B.G. Ghamsari, J. Abrahams, S. Remillard, S.M. Anlage, *Appl. Phys. Lett.* **102** (1), 013503 (2013)
- [57] J. Wu, B. Jin, Y. Xue, C. Zhang, H. Dai, L. Zhang, C. Cao, L. Kang, W. Xu, J. Chen, P. Wu, *Opt. Express* **19**, 12021 (2011)
- [58] A. Tsiatmas, V.A. Fedotov, F.J.G. de Abajo, N.I. Zheludev, *New Journal of Physics* **14**, 115006 (2012)
- [59] J. Zuo, R. Liu, Y. Zhou, Y. Li, Y. Wang, *Science China Physics, Mechanics and Astronomy* **55** (2), 224 (2012)
- [60] A.M. Zagoskin, *J. Opt.* **14**, 114011 (2012)
- [61] S.I. Mukhin, M.V. Fistul, arXiv:1302.5558v1 (2013)
- [62] R.D. Wilson, M.J. Everitt, S. Savelev, A.M. Zagoskin, *Supercond. Sci. Technol.* **26**, 084005 (2013)
- [63] P. Macha, G. Oelsner, J.M. Reiner, M. Marthaler, S. André, G. Schön, U. Hübner, H.G. Meyer, E. Il'ichev, A.V. Ustinov, arXiv:1309.5268v1 (2013)
- [64] N. Lazarides, G.P. Tsironis, *Supercond. Sci. Technol.* **26**, 084006 (2013)
- [65] N. Lazarides, V. Paltoglou, G.P. Tsironis, *Int. J. Bifurcation Chaos* **21**, 2147 (2011)
- [66] N. Lazarides, G.P. Tsironis, *Phys. Lett. A* **374**, 2179 (2010)
- [67] Y. Huang, W.F. McColl, *J. Phys. A: Math. Gen.* **30**, 7919 (1997)